Mechanical Behavior of Dou-Gong Brackets in Chinese Traditional Timber Structures: An Experimental Study

Ruyuan Yang,[a,b] Weidong Lu,[b,*] Longlong Zhao,[c] and Tao Li [a,b]

This study investigated the mechanical behaviour of Dou-Gong brackets with different structural forms, including Jixinzao and Touxinzao. Scaled Dou-Gong models were designed and fabricated at a 1:3.4 geometrical ratio. Vertical load tests were conducted to determine the failure modes, load-displacement response, stiffness degradation, and deformation capacity of the Dou-Gong models. Under vertical load, the primary failure modes of the Dou-Gong models were observed at the Lu-Dou, Nidao-Gong, and Hua-Gong component. The specimens demonstrated excellent load-bearing capacity and high deformation resistance. The Jixinzao Dou-Gong model exhibited a 15.0% higher ultimate load-carrying capacity than the Touxinzao Dou-Gong due to the presence of transverse arches. The number of transverse arches in the Dou-Gong models positively correlated with the compression stiffness, while their presence had a negligible effect on stiffness degradation rates. The Touxinzao Dou-Gong model exhibited superior ductility, characterized by a ductility coefficient 8.57% higher than that of the Jixinzao Dou-Gong model. Although the regular layering of the Dou-Gong models was disrupted by Ang component, the models remained stable in both the vertical and horizontal directions. The bi-linear model can effectively simulate the deformation behaviour of the Dou-Gong model under vertical load.

DOI: 10.15376/biores.18.4.7745-7768

Keywords: Traditional timber structure; Dou-Gong; Vertical loads; Failure modes; Mechanical properties

Contact information: a: College of Art & Design, Nanjing Tech University, Nanjing, 211816, P.R. China; b: College of Civil Engineering, Nanjing Tech University, Nanjing, 211816, P.R. China; c: College of Civil Engineering, Nanjing Forestry University, Nanjing, 210037, P.R. China;
**Corresponding author: ryyang@njtech.edu.cn*

INTRODUCTION

Different from modern steel structures, reinforced concrete structures, and modern timber structures connected by mechanical fasteners, Chinese traditional timber structures have their own structural characteristics, forming a unique architectural style in the world (Lu and Deng 2012; Gao *et al*. 2022; Xu *et al*. 2022). Among them, the Hall-type timber structure is one of the most complex structural forms with the highest class (Fig. 1). It plays an important role in the history of Chinese architecture (Liu *et al*. 2021; Yang *et al*. 2023).

The Dou-Gong bracket is a prominent feature of the Hall-type timber structure, and it is also a symbolic element of Chinese traditional architectural culture, reflecting the essence of Chinese traditional construction techniques. It consists of several components, including Dou, Gong, Ang, and others. As a key structural member of the traditional timber structure, the Dou-Gong bracket, plays an important role in transferring the load of the roof-beam system to the column frame layer. It serves both structural load-bearing and decoration functions, and its mechanical properties affect structural safety. Therefore, it is

of great significance to study the structural performance of Dou-Gong brackets for the protection of traditional timber structures. The structural decomposition of the Dou-Gong bracket can be shown in Fig. 2. It is worth noting that the horizontal direction, *i.e.* the orientation of Nidao-Gong and Hua-Gong, corresponds to the direction of the wood parallel to the grain.

(a) **(b)**

Fig. 1. The typical Hall-type timber structure: (a) the Hall of Saintly Mother of Jinci Memorial Temple in Shanxi Province; (b) the Main Hall of Kaishan Temple in Hebei Province

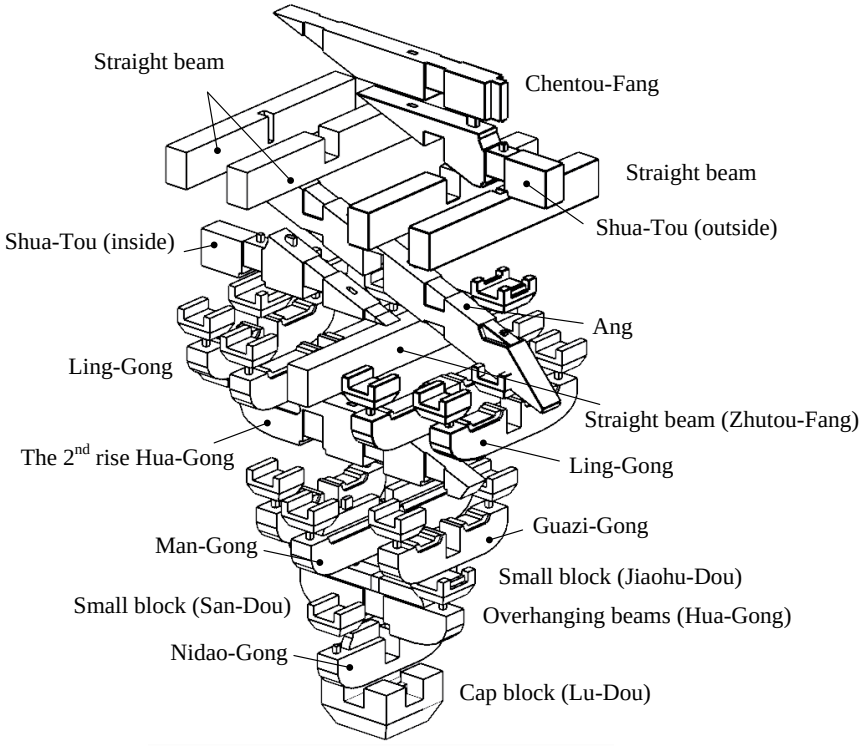

Fig. 2. Split graph of different components on Dou-Gong bracket

The Dou-Gong bracket underwent a gradual evolution, leading to an increase in the number of its components. From 206 B.C. to 479 A.D. (the Han Dynasty to the Northern and Southern Dynasties), the Dou-Gong bracket was exclusively comprised of Dou and transverse Gong components. At that time, Dou-Gong brackets did not have the function of making the eaves overhang longer. They only played the role of reducing the internal

force of the Yanling (eave purlin). Later, the emergence of Hua-Gong (overhanging beams) and Ang required that the Dou-Gong bracket also take on the function of overhanging eaves. Throughout the Tang Dynasty to the Yuan Dynasties, which spanned from 618 to 1368 A.D., the Dou-Gong bracket underwent significant development, resulting in the establishment of a comprehensive system. Based on the roles and functions of the Dou-Gong bracket in the structure, it can be divided into three categories, *i.e.*, column set (Dou-Gong bracket at column top), corner set (Dou-Gong bracket at the corner), and intermediate set (Dou-Gong bracket at intermediate position). Moreover, the structural form of the Dou-Gong bracket differs between Jixinzao (Dou-Gong bracket with transverse arch) and Touxinzao (Dou-Gong bracket without transverse arch) (Pan 2004).

The two structural forms of the Dou-Gong bracket described above were extensively discussed in the book *Yinzao Fashi (Building Regulation)* (Li 1982) published by the Northern Song Dynasty government in 1103 A.D. It is reported that Hua-Gong and Ang as the longitudinal components that project outward in the Dou-Gong bracket. In the Jixinzao structural form of the Dou-Gong bracket, the transverse arch is typically positioned above the Hua-Gong and Ang, while in the Touxinzao structural form, the San-Dou is placed on the Hua-Gong and Ang without the transverse arch. The Dou-Gong bracket at the top of the column in the East Hall of Foguang Temple is a representative Dou-Gong structure of the Chinese Tang Dynasty, and the differences between the two construction methods are illustrated in Fig. 3. From 1368 to 1912 A.D., corresponding to the Ming and Qing Dynasties, a gradual increase in the number of transverse arches on both the Hua-Gong and Ang was implemented. This adjustment was made with the primary objective of enhancing the overall structural stability. Consequently, the structural configuration of the Dou-Gong bracket underwent a gradual transformation, transitioning from the Touxinzao to the Jixinzao form.

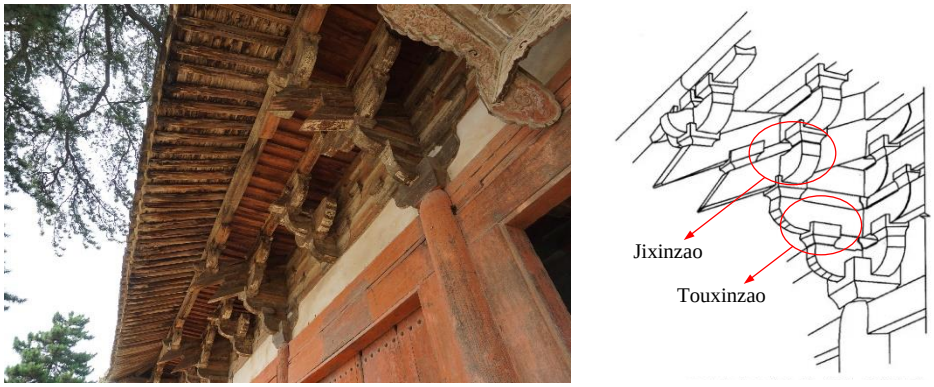

Fig. 3. The Dou-Gong bracket at column top in the East Hall of Foguang Temple: (a) exterior photo; (b) the structural form of Jixinzao and Touxinzao Dou-Gong bracket

Wood exhibits a series of advantages, including energy conservation, environmental friendliness, high strength-to-weight ratio, as well as cost effectiveness. However, it also possesses anisotropic properties, thus introducing complexity to its mechanical behavior. In recent decades, several scholars have conducted extensive studies on the mechanical properties of the Dou-Gong bracket. Zhou *et al*. (2015, 2017) conducted experimental studies on three different types of Qing-style Dou-Gong bracket in the first and second floors of the Taihe Hall of the Forbidden City. The failure modes, internal

forces, and deformation characteristics of different Dou-Gong brackets under vertical load were discussed, and the vertical stiffness calculation model of the Dou-Gong bracket was investigated. Liu *et al*. (2020a,b) used the Dou-Gong bracket between the columns of the Main Hall of Huishan Temple as the research object and fabricated the full-scale model specimens. Through the vertical monotonic load test, the deformation capacity and force transmission mechanism of the Dou-Gong bracket under the vertical load were considered, and the mechanical model of the vertical bearing capacity was obtained. Test results showed that under the vertical load, shear, and load-bearing failure were easy to occur at the intersection of Lu-Dou, Ang, and Nidao-Gong, which was the weak part of the Dou-Gong bracket. The ultimate bearing capacity of the Dou-Gong bracket was about 383 kN, and the residual deformation was about 22.3 mm, which showed the good vertical bearing and deformation capacity of the Dou-Gong bracket. The vertical stiffness calculation model of the Dou-Gong bracket in the Main Hall of Huishan Temple can be simplified to the trilinear model under the vertical load. Yeo *et al*. (2016, 2018) carried out pseudo-static tests on Taiwanese traditional Dieh-Dou timber structures. The load-displacement relationship of the Dieh-Dou timber structure under the vertical and horizontal loads was obtained, and a hysteretic model was established. Wang (2016) simulated the mechanical properties of the Jixinzao and Touxinzao Dou-Gong bracket under the vertical static load and the horizontal low-cycle repeated load by the finite element (FE) software, and obtained the calculation models of the Dou-Gong bracket. The results showed that the vertical ultimate bearing capacity and lateral stiffness of Jixinzao Dou-Gong bracket is better compared with the Touxinzao Dou-Gong bracket, and the Jixinzao Dou-Gong bracket is more beneficial to the seismic energy consumption of traditional timber structures than the Touxinzao Dou-Gong bracket. Pan *et al*. (2017) used the Jixinzao and Touxinzao Dou-Gong bracket of the Great Buddha Hall of Raoyi Temple as the research object and established the finite element models (FEM), the mechanical properties of the two kinds of Dou-Gong brackets under vertical load and horizontal low-cycle repeated load were analyzed. The results showed that under the vertical load, the Jixinzao Dou-Gong bracket experienced a strength hardening stage, with the ultimate bearing capacity 29.9% higher than that of Touxinzao Dou-Gong bracket, and the additional structural member (transverse arch) in Jixinzao Dou-Gong bracket contributed to the higher bearing capacity. Under the horizontal low-cycle repeated load, the two kinds of Dou-Gong brackets behaved equally well in terms of energy dissipation performance, and both exhibited relatively plump hysteresis loops.

To date, existing research has primarily focused on the mechanical properties of Dou-Gong brackets fabricated according to the book of *Yinzao Fashi (Building Regulation)* (Li 1982) or some Dou-Gong brackets in typical northern official traditional structures of the Ming and Qing dynasties. However, the quantitative influence of the structural form on the structural performance of the Dou-Gong bracket has been relatively limited, with a lack of systematic theoretical and experimental research. This study presents the results of an experimental investigation into the structural performance of two Dou-Gong models *i.e*. Jixinzao Dou-Gong model DG-1 and Touxinzao Dou-Gong model DG-2, with a geometrical ratio of 1:3.4 under monotonic static vertical load. The structural performance of the Dou-Gong bracket in terms of failure modes, load-carrying capacity, stiffness, and ductility was investigated. Through this work, the evolution of the Dou-Gong bracket from the perspective of mechanics is interpreted, and the results can serve as a reference for the protection and maintenance of Chinese traditional timber structures.

EXPERIMENTAL

Materials

The selection of materials for Chinese traditional timber structures follows the principle of "utilizing local and nearby materials". Building materials for Chinese traditional timber structures often include widely distributed wood species such as pine (*Pinus* sp.), China fir (*Cunninghamia* sp.), cedarwood (Cupressaceae), and poplar (*Populus* sp.). For example, in the Yingxian Wood Pagoda in Shanxi Province, larch (*Larix gmelinii*) is mostly used as the timber frame material, and in the Main Hall of Beiyue Temple in Hebei Province, spruce (*Picea asperata*) is used as the column material (Ni and Li 1994, Yuan *et al*. 2021). In this study, *Pinus sylvestris* was used as the model material, which was obtained from the same batch of logs to minimize the effects of various factors, including wood density, moisture content, and maturity, on the mechanical properties of the material. Material tests were conducted on the raw material following ASTM D143 (2014), GB/T 1931 (2009), and GB/T 1933 (2009). The basic material properties are listed in Table 1.

Table 1. Basic Properties of *Pinus sylvestris*

Wood species	$E_{//}$/MPa	$E_{\perp}$/MPa	$f_{c//}$/MPa	$f_{c\perp}$/MPa	ρ/(g·cm^{-3})	*MC*/%	Number of specimens
Pinus sylvestris	9870 (0.1651)	258 (0.1984)	37.60 (0.0729)	6.13 (0.0870)	0.44 (0.0361)	11.86 (0.0313)	20

Notes: The value in parentheses denotes the coefficient of variation. In the table, E_i denotes the elastic modulus (MPa); f_c denotes the compression strength under all-area compression (MPa); The subscript // and ⊥ denote the direction parallel to the grain and perpendicular to the grain, respectively; ρ denotes the air-dried density (g·cm^{-3}); *MC* denotes the moisture content (%).

Fabrication of Specimens

Considering that the structural form and dimension of the Dou-Gong bracket are closely related to the class and function of the building, the Chinese Song-style Dou-Gong bracket with Ang was selected as the prototype in the current study, based on relevant literature (Li 1982; Chen 1991; Wang 1992).

Table 2. The Conversion Method for the Sectional Dimensions of Wood Used During the Song Dynasty

Unit		First class	Second class	Third class	Fourth class	Fifth class	Sixth class	Seventh class	Eighth class
Song Dynasty	Height (cun)	9	8.25	7.5	7.2	6.6	6	5.25	4.5
	Width (cun)	6	5.5	5	4.8	4.4	4	3.5	3
Metric system	Height (mm)	278	255	232	222	204	185	162	139
	Width (mm)	185	170	155	148	136	124	108	97

Note: In the unit system of the Song Dynasty, 1 cun was converted to 30.9 to 32.9 mm in metric system, and 30.9 mm is taken in the current study.

Initially, the wood used to fabricate the prototype Dou-Gong bracket underwent cutting with a band saw, resulting in cross-sectional dimensions of 255 mm × 170 mm

(height × width), and the conversion method for the sectional dimensions of wood used during the Chinese Song Dynasty is presented in Table 2. Subsequently, skilled carpenters meticulously crafted each component by hand. Lastly, the bracket was meticulously polished to a smooth finish using sandpaper.

In light of the potential machining and assembly errors, two Dou-Gong models with a geometrical ratio of 1:3.4, *i.e.*, the Jixinzao Dou-Gong model DG-1 and Touxinzao Dou-Gong model DG-2 were fabricated. The overall geometry of the 1:3.4 scale Dou-Gong model is characterized by dimensions of 450 mm × 840 mm × 490 mm in height, length (Hua-Gong direction) and width (Nidao-Gong direction), respectively, as shown in Fig. 5.

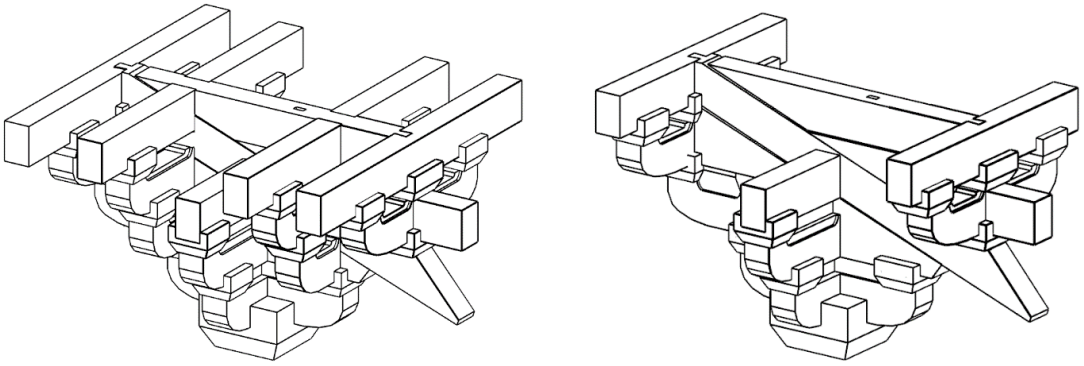

Fig. 4. Schematic diagram of Dou-Gong brackets: (a) the Jixinzao Dou-Gong model DG-1; (b) the Touxinzao Dou-Gong model DG-2

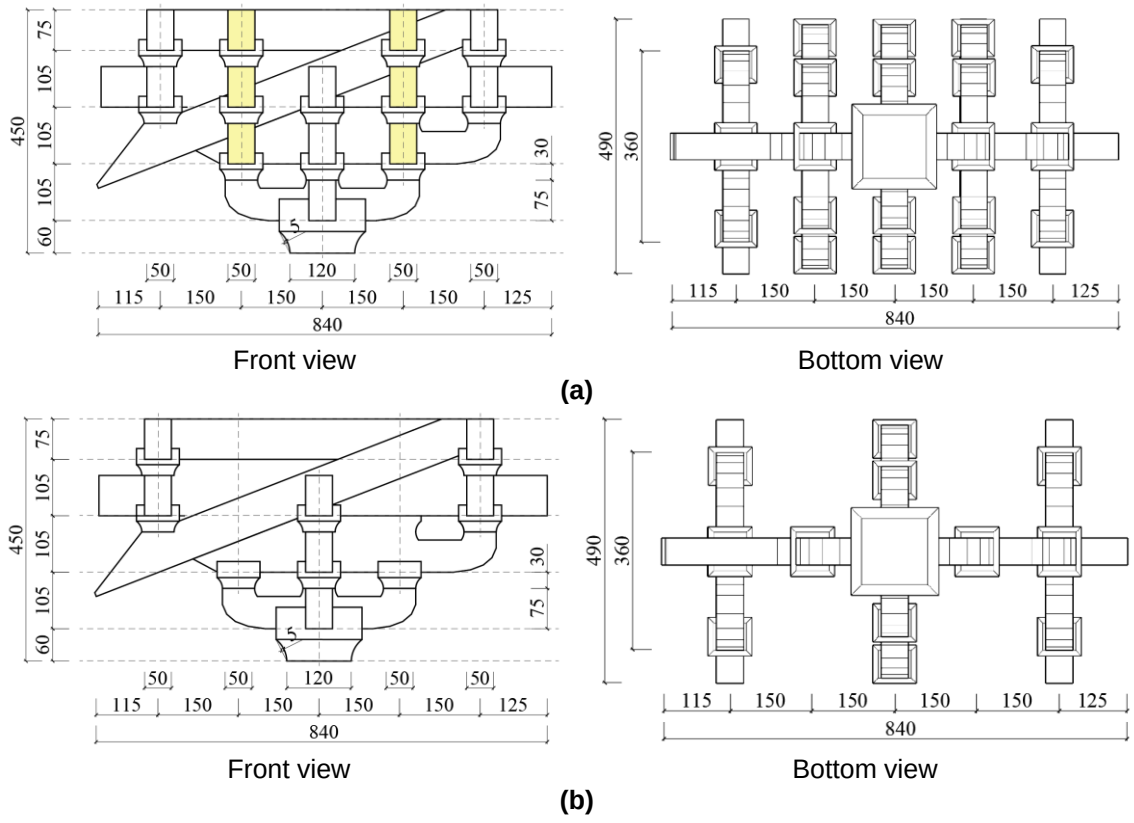

Fig. 5. Dimensions of Dou-Gong models (all dimensions are in mm): (a) specimen DG-1; (b): specimen DG-2

The prototype Dou-Gong bracket comprises components manufactured based on a dimension module of a_p = 17 mm, as specified the book of *Yinzao Fashi (Building Regulation)* (Li 1982). Therefore, the dimensions of the wood used to fabricate the 1:3.4 scale Dou-Gong model are multiples of a_s = 17/3.4 = 5 mm. Specifically, the Lu-Dou has dimensions of 20*a* × 32*a* × 32*a* (height × length × width), and the Hua-Gong has dimensions of 21*a* × 72*a* × 10*a* (height × length × width). More detailed dimensional information on Dou-Gong components can be seen in Fig. 6. The cross-sectional dimension of other Gong and Fang is 15*a* × 10*a* (height × width), and the overall geometry dimensions of Jiaohu-Dou and San-Dou are 10*a* × 18*a* × 16*a* (height × length × width) and 10*a* × 14*a* × 16*a* (height × length × width), respectively. To connect partial components of the Dou-Gong model, hidden timber dowels with dimensions of 4*a* × 2*a* × 2*a* (height × length × width) are utilized. All internal hidden structures of the components, such as the slotting, are fabricated in accordance with the guidelines presented in the book of *Yinzao Fashi* (Li 1982) and relevant literature (Pan 2004).

The Dou-Gong bracket comprises numerous small components with a complex manufacturing process, as illustrated in Fig. 6. To economize on testing expenditures, a cost-efficient strategy that involved the replacement of failed components after each test was used. This method commenced with the disassembly of all Dou-Gong bracket components following testing. Subsequently, a meticulous inspection of each component took place, with particular attention devoted to averting any minor damage that might potentially compromise the mechanical performance of the Dou-Gong bracket. Finally, the failed components were substituted, and the Dou-Gong model was reassembled. This systematic method enabled the execution of three repeated tests for each Dou-Gong model. It should be noted that the Dou-Gong bracket serves both structural and decorative purposes. To simplify the manufacturing process, the decorative components that do not impact the structural performance were omitted in the current study, and the main simplified parts were as follows: (1) the Juan-Sha (the end of the component made into an arc shape) was replaced with a chamfer, and the volume of wood removed by both methods was equal; (2) the bottom of all types of Dou was cut into a pyramid-shaped frustum without making radians; (3) the Qinmian-Ang at the end of the Ang was simplified to a straight Pizhu-Ang. Each component was prefabricated in the factory and then assembled in the laboratory.

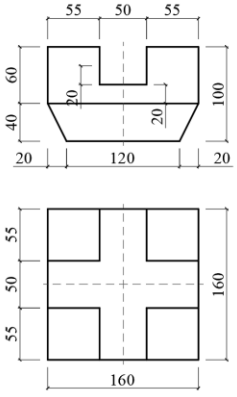

(a) Cap block (Lu-Dou)

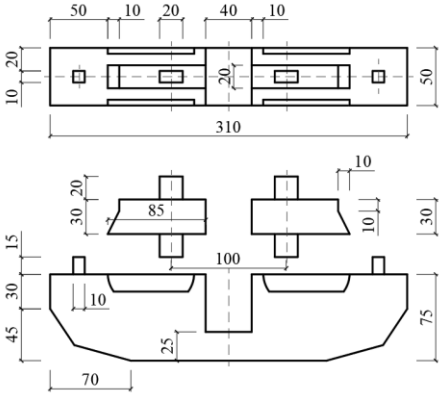

(b) Nidao-Gong

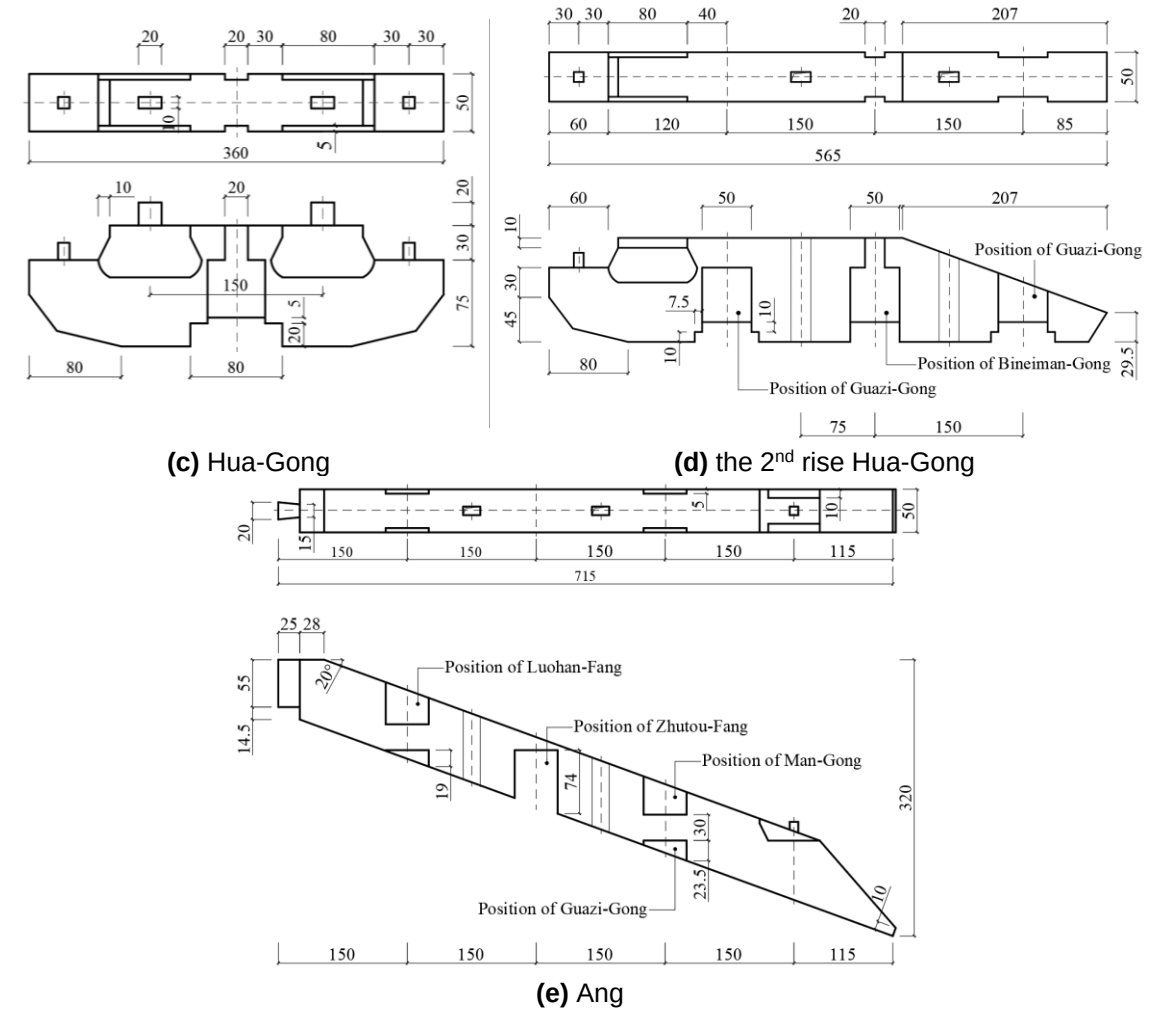

(c) Hua-Gong **(d)** the 2nd rise Hua-Gong

(e) Ang

Fig. 6. Dimensions of partial components (all dimensions are in mm)

Arrangement of Measurement Points and Loading Protocol

Loading protocol

During the test, the Dou-Gong models were installed upside down on the steel base, and the geometric center of the loading block passed through the central points of Lu-Dou, which ensured that the vertical load was applied along the central axis of the Dou-Gong models. All ends of the Gong components were free from any restriction. To minimize the impact of uneven stress on displacement measurement, silver sand was used to ensure that the bottom surface of the Dou-Gong model had uniform contact with the testing platform. The test setup is illustrated in Fig. 7.

Under vertical load, the load-displacement curve of the Dou-Gong bracket showed similarity to that of wood under compression perpendicular to the grain without a clearly defined ultimate load. Therefore, the displacement-controlled loading method was employed in the current study. The Dou-Gong models were loaded as follows: (1) Initially, the preload was applied to reduce the assembly clearance. According to the research conducted by Gao *et al*. (2003), the internal force and deformation of the Dou-Gong bracket do not exceed 1/7 of its ultimate strength in the normal use stage, and it is always in the elastic stage. Therefore, the preload was increased to 8 kN for the Jixinzao Dou-Gong model DG-1, and 5 kN for the Touxinzao Dou-Gong model DG-2, respectively; (2)

During the formal loading, the load was applied with a displacement rate of 1 mm·min^{-1} until some components of the Dou-Gong model either yielded or fractured. At this point, the Dou-Gong model was visibly damaged, yet the load-displacement curve continued to ascend with a smaller slope; (3) During the unloading stage, the unloading rate was maintained at 10 kN·min^{-1}. The corresponding residual deformation of each specimen was recorded after unloading to 0. The laboratory temperature was 14 ± 3 °C, and the relative humidity was 58 to 65%. The entire test was conducted in a stable environment.

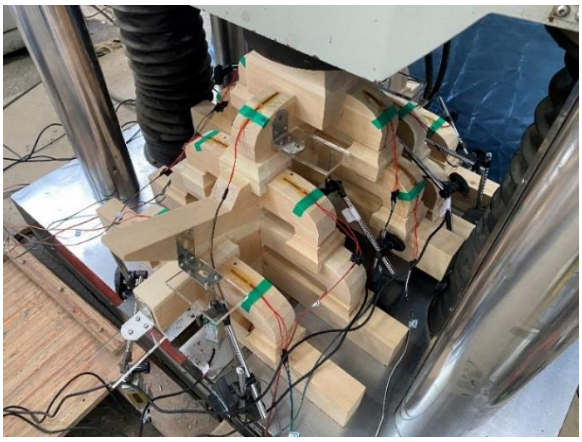

Fig. 7. Set up used for testing Dou-Gong models (taking DG-1 as an example)

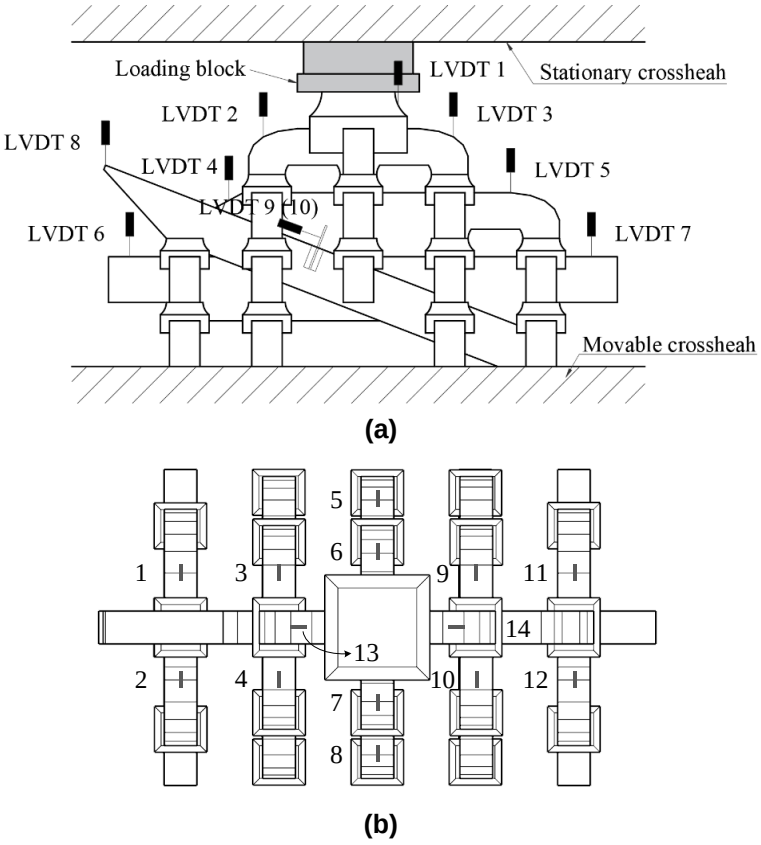

Fig. 8. Loading and measurement of displacement and strain for testing Dou-Gong models: (a) Layout of displacement meters; (b) Layout of strain gauges

Test configurations and setup

The applied load was quantified using a load senser positioned at the top of Dou-Gong models. Vertical displacements of specific components were recorded using eight displacement meters (model: YHD-50, China), designated as LVDT 1 to 8. These were positioned to measure the displacements of Lu-Dou (LVDT 1), the end of Hua-Gong (LVDT 2 and 3), the 2nd rise Hua-Gong (LVDT 4 and 5), Shua-Tou (LVDT 6 and 7), and Ang (LVDT 8). An additional two displacement meters (model: YHD-30, China), designated as LVDT 9 and 10, were installed at the interfaces between the 2nd rise Hua-Gong and Ang to detect any relative slip due to the applied loading. The arrangement of LVDTs is illustrated in Fig. 8(a). Strain measurements were obtained using fourteen electrical resistance strain gauges (model: BX120-30AA, China) placed at specific locations on Nidao-Gong, Hua-Gong, Bineiman-Gong, Guazi-Gong, and Ling-Gong (as indicated by the black stripe in Fig. 8b). All experiments were performed using a microcomputer-controlled electro-hydraulic servo universal testing machine with a capacity of 2000 kN (model: SAN SHT4 206, China) and a data acquisition system (model: TDS-530, Japan).

RESULTS AND DISCUSSION

Failure Modes

The Jixinzao Dou-Gong model DG-1

The study investigated short-term load-displacement behaviour of Dou-Gong models. Initially, the Dou-Gong model DG-1 was compacted at a vertical displacement of approximately 2.18 mm, influenced by the processing accuracy of components. As the load increased to approximately 15 kN, a squeak was heard at the clearance of components due to the biting force between them, while no significant cracking was observed in other components. With continued loading, the Lu-Dou cracked (at a load of around 25 kN) at the corner of the precut slots, *i.e.*, the root of a protuberance, and the crack gradually widened. Simultaneously, splitting cracks appeared on the end of Hua-Gong and Nidao-Gong, extending from the position of Juan-Sha to the intersection with the Lu-Dou, as shown in Fig. 9(a). At around 40 kN, the wood fibers at the surface of Hua-Gong tilted upwards, accompanied by frequent splitting sounds (Fig. 9b). Subsequently, the Lu-Dou collapsed at approximately 72 kN, and the protuberance on one side was almost severed from the root (Fig. 9c). Due to the local bending moment caused by the concentrated force, an accompanied uplift (Fig. 9d) of the far end of the Nidao-Gong was also observed. The cracks on the Nidao-Gong and Hua-Gong gradually developed into a through crack, and the splitting sound became low frequency and high-pitched. At a load of approximately 82 kN, the bending deformation of the Nidao-Gong was more evident, and the tenon pulling phenomenon occurred at both ends. The Nidao-Gong and Hua-Gong split at the intersection with the Lu-Dou (Fig. 9e). Finally, the loading was terminated due to excessive deformation, and no further decrease in stiffness was observed. At this point, the relative slip between the Ang and the 2nd rise Hua-Gong was small, not exceeding 1 mm. During unloading, the components with bending deformation tended to recover. The Dou-Gong model produced a dense sound caused by the loose bite between components as the load decreased.

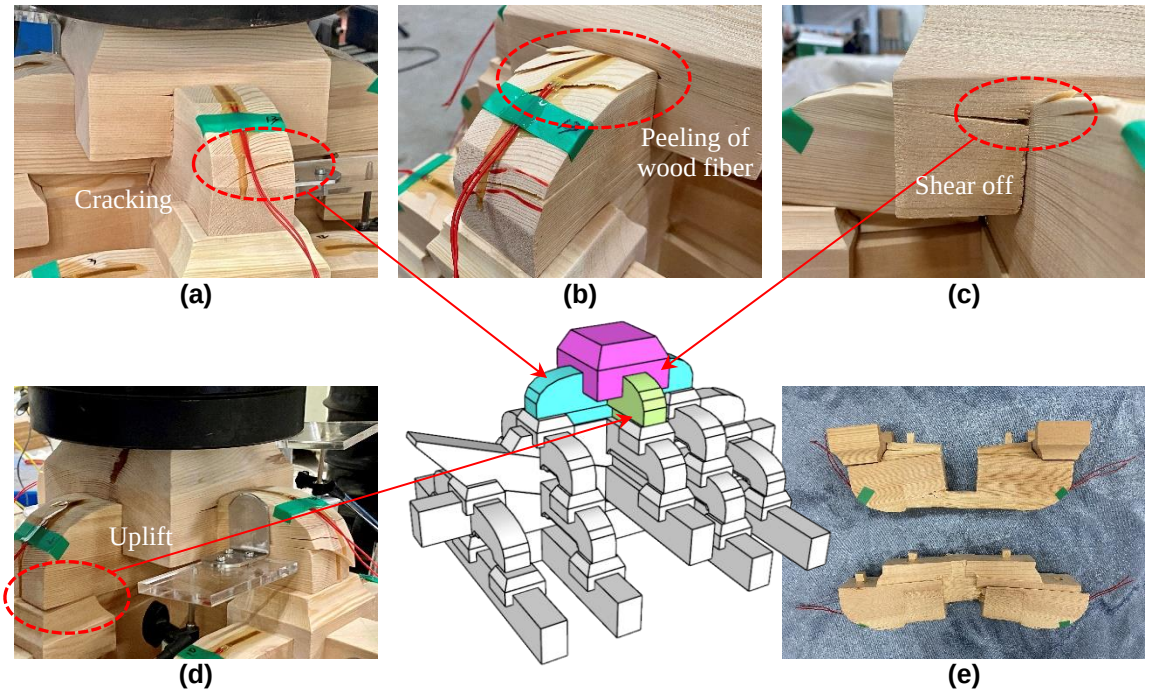

Fig. 9. Typical failure modes of specimen DG-1: (a) Hua-Gong cracked; (b) peeling of wood fiber; (c) Lu-Dou cracked at the root of a protuberance; (d) bending deformation of Nidao-Gong; (e) Nidao-Gong and Huagong yielded locally and fractured

The damage of the model DG-1 was primarily concentrated on the Lu-Dou, Nidao-Gong, and Hua-Gong components, while the other components remained intact without obvious deformation. The Dou-Gong model DG-1 exhibited three failure modes, which were identified as: (i) yield of Lu-Dou, Nidao-Gong, and Hua-Gong under compression perpendicular to the grain; (ii) cracking of Lu-Dou, Nidao-Gong and Hua-Gong under tension perpendicular to the grain; and (iii) shear failure of Nidao-Gong and Hua-Gong. The yield and cracking of the components were the result of multiple micro-deformation that slowly accumulated over time.

The Touxinzao Dou-Gong model DG-2

The mortise-tenon joint is a semi-rigid connection method that combines timber components through concave and convex parts, effectively limiting relative slip between components under loading. In the Dou-Gong model DG-2, there are fewer transverse arches, and the combination of components is not as tight as in model DG-1. At a vertical displacement of approximately 3.16 mm, the model DG-2 was essentially compacted. As the load increased to approximately 13 kN, the Dou-Gong model emitted a noticeable creaking sound, and no obvious deformation of each component was observed. Subsequently, the Nidao-Gong and Hua-Gong components displayed bending deformation at a load around 20 kN. Additionally, local plastic embedding deformation was observed on the surface of the Lu-Dou, with the protuberance gradually uplifting outward. At approximately 30 kN, a longitudinal crack appeared on the Nidao-Gong, beginning from the intersection with the Lu-Dou and extending to the end of the Nidao-Gong (Fig. 10a). Simultaneously, the Lu-Dou cracked perpendicular to the wood grain near the protuberance due to stress concentration at the precuts, as shown in Fig. 10(b). At approximately 43 kN, bending deformation of the Nidao-Gong and Hua-Gong was observed (Fig. 10c). At this

point, a relatively apparent relative slip between the Ang and the 2nd rise Hua-Gong was observed, as shown in Fig. 10(d). As the load increased to approximately 60 kN, 45-degree diagonal cracks appeared on the surface of the end of the Hua-Gong, with a crisp sound. The intersection of the Nidao-Gong and Hua-Gong experienced yield failure, and the Hua-Gong broke off due to combined shear and bending forces at approximately 72 kN (Fig. 10e). After loading, deformation was clearly observed on the Lu-Dou, Nidao-Gong, and Hua-Gong components, similar to DG-1 but with more components yielding. In contrast, the cracks at the end of the Nidao-Gong and Hua-Gong in DG-2 were notably fewer than those in DG-1. Additionally, the Jiaohu-Dou placed on the Shua-Tou cracked due to the relative slip of the Ang in the Dou-Gong model DG-2, and the hidden dowel on the Ang deformed. During the unloading process, at a load of approximately 16 kN, a "bang" was emitted from the specimen due to component deformation recovery.

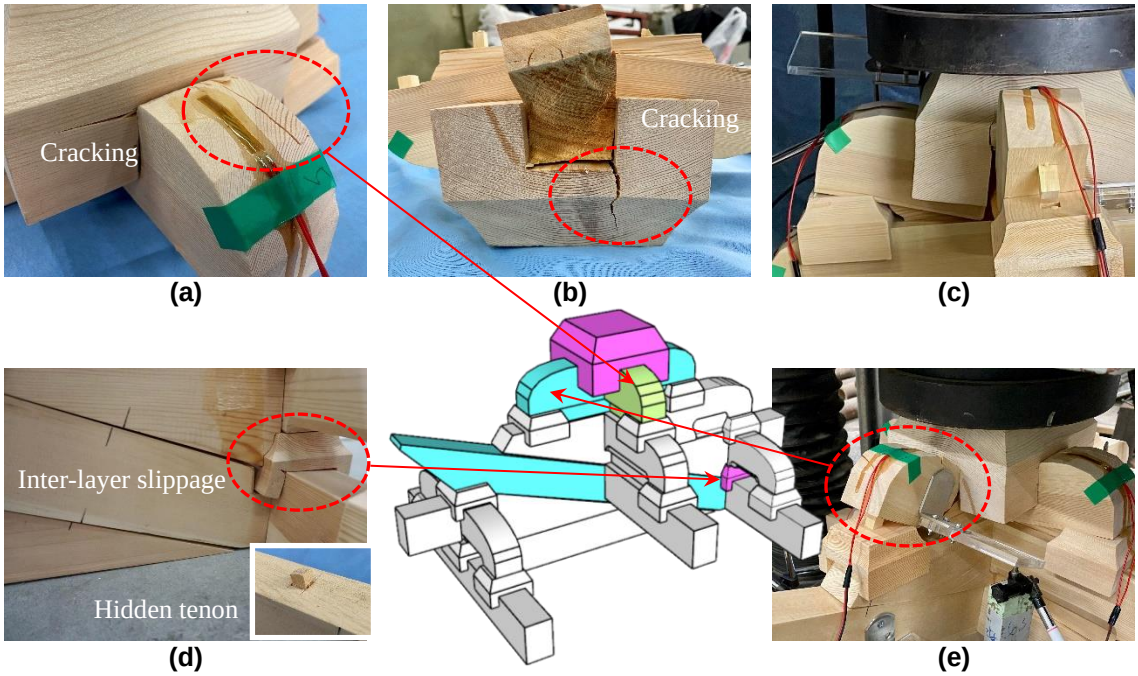

Fig. 10. Typical failure modes of specimen DG-2: (a) Hua-Gong cracked; (b) Lu-Dou cracked; (c) bending deformation of Nidao-Gong and Hua-Gong; (d) inter-layer slippage of Ang; (e) breaking-off of Hua-Gong

Four failure modes of the Dou-Gong model DG-2 were identified. These modes included (i) yield of Lu-Dou, Nidao-Gong, and Hua-Gong under compression perpendicular to the grain; (ii) cracking of Lu-Dou, Nidao-Gong, and Hua-Gong under tension perpendicular to the grain; (iii) shear failure of Lu-Dou, Nidao-Gong, Hua-Gong, Jiaohu-Dou, and Ang; and (iv) breaking-off of Hua-Gong under bending.

Comparison with related literature

Chen *et al*. (2014) conducted an experimental study on the structural performance of Dou-Gong brackets in Yingxian Wood Pagoda, and the test model was manufactured using Northeast China red pine (*Pinus koraiensis*) with a geometrical ratio of 1:3.4. Yield of Lu-Dou, and fractures of Nidao-Gong and Hua-Gong were observed during their tests, which were similar to the failure modes of components of DG-1 (Fig. 9e) and DG-2 (Fig. 10a and 10e). Xue *et al*. (2022) investigated the vertical mechanical performance of the

Dou-Gong at column tops through a vertical monotonic loading test and numerical simulation. The failure observations of their compression specimens were cracks of Lu-Dou, Nidao-Gong, and Hua-Gong, similar to DG-1 (Fig. 9a-d) and DG-2 (Fig. 10a-b). Cheng *et al*. (2019) fabricated 1:3.52 scaled China fir models of Song-style Dou-Gong brackets at the column top with Ang and carried out vertical load tests, showing that Lu-Dou was the first to be destroyed under different loads.

These studies serve as validation for the current study, which establishes that the transmission of vertical loads in the Dou-Gong bracket occurs sequentially from top to bottom, utilizing the following components: Shua-Tou, Ang, Hua-Gong, Nidao-Gong, San-Dou, and Lu-Dou. Due to the gradual increase in internal force from top to bottom, Lu-Dou is more susceptible to crushing and splitting failures as a weak member compared to other components of the Dou-Gong bracket. In future research endeavors, an intriguing and promising avenue for exploration resides in the enhancement of the mechanical performance of the Dou-Gong bracket through the reinforcement or alteration of the dimensions of these vulnerable components.

Load-displacement Response

The vertical displacement of the Dou-Gong model is the sum of two parts *i.e.* stress deformation of each component in the vertical direction and compression deformation of the assembly clearance between the components in each layer. This composite displacement reflects the overall vertical compression deformation characteristics of the Dou-Gong model and can be simplified as the vertical displacement of the actuator. The load-displacement curves of the tested Dou-Gong model are presented in Fig. 11 and can be divided into four distinct stages.

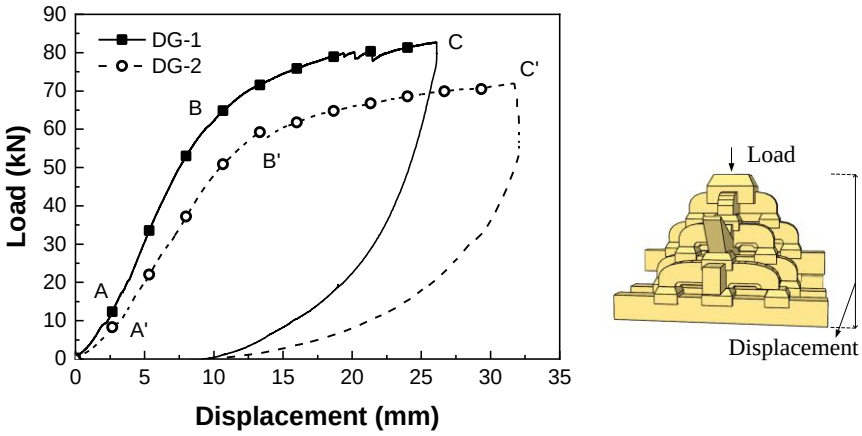

Fig. 11. Load-displacement curves for specimens

The first stage was the initial compaction stage (OA segment), which was characterized by low stiffness due to incomplete contact between components resulting from fabrication errors and assembly clearance. At 9.31 kN and 9.42 kN for DG-1 and DG-2, respectively (*i.e.*, the A point), displacement development slowed down due to components deforming under compression perpendicular to the grain. The second stage was the elastic stage (AB segment), where the recorded displacement developed at a rate almost proportional to the increase in loading. The third stage, starting from the end of the second stage up to the ultimate loading point (*i.e.*, the C point), was characterized by a non-linear load-displacement response. As the load increased, the displacement of the Dou-

Gong models accelerated, while the rate of load increase was significantly reduced. The vertical compression stiffness was rapidly reduced, and the Dou-Gong exhibited characteristics of plastic deformation with increased deformation. The specimens reached their limit state when the Lu-Dou, Nidao-Gong, and Hua-Gong components were evidently damaged. The fourth stage was the unloading stage, during which the rate of displacement recovery in the early stage was lower than that of load reduction. The deformation recovery of the Dou-Gong model was not immediately evident at this stage, but gradually accelerated. Except for the early OA segment and unloading stage, the structural characteristics of the Dou-Gou model were similar to those of wood under compression perpendicular to the grain.

The parameters of yield load F_y, peak load F_{max} and ultimate load F_u were established using the load-displacement curves of Dou-Gong models. F_y was described as the vertical load at which the vertical compression stiffness of the Dou-Gong model experiences significantly changes, F_{max} represents the maximum load attained during the loading process, while F_u was identified as the load that resulted in specimen damage. The results presented in Fig. 11 indicate that both DG-1 and DG-2 had equal F_{max} and F_u values, indicating that the bearing capacity of each Dou-Gong model did not decrease during the loading process. This observation implies that Dou-Gong models can maintain their overall bearing capacity even after experiencing large displacement under short-term load, despite damage to individual components. It further highlights the strong deformation ability of the Dou-Gong bracket, emphasizing that displacement control is a more reasonable method in engineering design. Nevertheless, the creep of wood can significantly affect the deformation of the structure, particularly the long-term bearing capacity of the Dou-Gong bracket (Zheng *et al*. 2023). Therefore, future research should explore this aspect.

Upon comparing the structural performance of DG-1 and DG-2 under vertical load, it was observed that both Dou-Gong models displayed notable bearing capacity. Specifically, DG-1 and DG-2 exhibited ultimate loads of 82.8 kN and 72 kN, respectively, with DG-1 showing a 15.0% higher ultimate load than DG-2. Additionally, DG-1 exhibited a yield load that was 18.4% higher than that of DG-2. This difference in performance is ascribed to the greater number of transverse arches present in the Jixinzao Dou-Gong model DG-1, which serves to augment its overall structural integrity and, in turn, enhance its bearing capacity.

Degradation of Compressive Stiffness

Throughout the loading process, the load-displacement curve exhibits three stages with varying stiffness levels.

Table 3. Key Test Results Obtained for All Specimens

Group No.	F_u/kN	F_y/kN	K_{OA}/(kN·mm^{-1})	K_{AB}/(kN·mm^{-1})	K_{BC}/(kN·mm^{-1})	ξ/%
DG-1	82.78	69.33	4.48	6.94	0.97	86.02
DG-2	72.00	58.53	3.19	5.42	0.76	85.98

Notes: In the table, F_u denotes the ultimate load (kN), which is directly obtained from test data; F_y denotes the yield load (kN), which is determined using the general yield moment method outlined by Fan and Zhuo (2001); K_{OA} denotes the secant stiffness corresponding to the OA segment (kN·mm^{-1}); K_{AB} denotes the secant stiffness corresponding to the AB segment (kN·mm^{-1}); K_{BC} denotes the secant stiffness corresponding to the BC segment (kN·mm^{-1}); ξ denotes the degradation rate of compressive stiffness, $\xi = [(K_{AB} - K_{BC})/K_{AB}] \times 100\%$

The vertical compression stiffness of the Dou-Gong model was assessed through regression analysis, which involved calculating the tangential slope of each loading segment, including the vertical stiffness K_{OA} in the initial stage (OA segment), the vertical stiffness K_{AB} in the elastic stage (AB segment), and the vertical stiffness K_{BC} in the elastic-plastic stage (BC segment). The primary mechanical performance parameters for each specimen were assessed by computing the mean value for each group of specimens, as summarized in Table 3.

Figure 12 presents the results of the regression analysis of the load-displacement curves, which demonstrate a remarkable level of agreement between the fitted curve and test data. Notably, the elastic range of the curve (AB segment) shows a high determination coefficient R^2 value of 0.99, indicating a high level of precision in the fitting process. These findings highlight the significant accuracy achieved in the regression analysis of the load-displacement curves. The preloading successfully eliminated some looseness as the stiffness from the subsequent loading was noticeably increased. Furthermore, the compression stiffness of the Dou-Gong model DG-1 in the two loading segments was greater than that of DG-2 in both cases. In the elastic stage, DG-2 exhibited a stiffness that was 21.9% lower than DG-1, with a similar reduction of 21.6% observed in the elastic-plastic stage, suggesting that compression stiffness is augmented with an increase in the number of transverse arches. However, the vertical stiffness degradation rates of DG-1 and DG-2 were observed to be relatively similar, with a decrease of 86.0% and 86.0%, respectively, in compression stiffness between the elastic and elastic-plastic stages, indicating that the presence of transverse arches has a negligible effect on stiffness degradation rates.

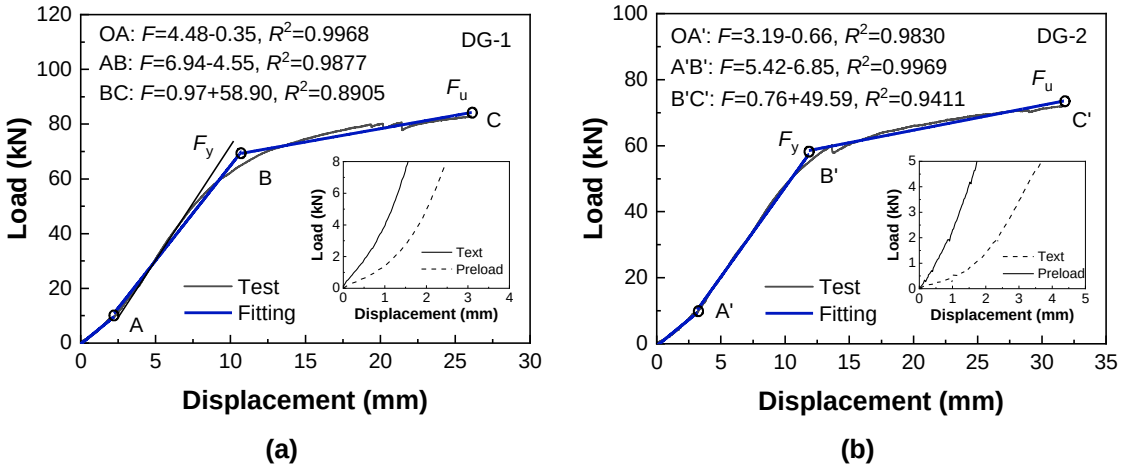

Fig. 12. Vertical load-displacement curves and fitting results: (a) Fitting results of specimen DG-1; (b) Fitting results of specimen DG-2

Ductility and Residual Deformation

Under external loading, the Dou-Gong model exhibited an increase in deformation and eventual yielding, while retaining its bearing capacity, indicating a certain level of ductility. The ductility coefficient *D* quantifies the continuous bearing capacity of the specimen after yielding (Yang *et al*. 2020). A higher value of the ductility coefficient reflects a stronger bearing capacity of the Dou-Gong model after yielding. The ductility coefficient *D* can be determined according to Eq. 1,

$$D = \frac{\Delta_u}{\Delta_y} \quad (1)$$

where Δ_u denotes the compression deformation corresponding to the ultimate load (mm); and Δ_y denotes the compression deformation corresponding to the yield load (mm).

Table 4 presents the ultimate displacement Δ_u, residual deformation Δ_R, and ductility coefficient D of each specimen. Both Dou-Gong models demonstrate favorable deformation capacity, particularly with respect to inelastic deformation capacity under vertical load. Liu *et al*. (2020a) arrived at a concordant conclusion. Their findings indicated that the ductility coefficient D of the Dou-Gong bracket under vertical load amounted to 8.34, while the ductility coefficient under horizontal load was 5.11, illustrating a commendable degree of ductility. In the current study, the Touxinzao Dou-Gong model DG-2 exhibits superior ductility, with a ductility coefficient 8.57% higher than that of the Jixinzao Dou-Gong model DG-1, indicating a more robust bearing capacity after yielding.

Table 4. Ultimate Displacement and Residual Deformation of Dou-Gong Brackets

Group No.	Δ_u/mm	Δ_y/mm	Δ_r/mm	D	η/%
DG-1	26.10	10.65	9.24	2.45	35.40
DG-2	31.67	11.97	12.12	2.66	38.27

Notes: Δ_r denotes the residual deformation (mm); D denotes the ductility factor; η denotes the residual deformation rate, $\eta = \Delta_r / \Delta_u$.

The residual deformation of the Dou-Gong model can be decomposed into two parts, *i.e.*, the plastic deformation of the wood and the permanent deformation caused by the clearance that has not been restored after compression. In the aftermath of the test, the residual deformation of DG-1 and DG-2 models were found to be 9.24 mm and 10.53 mm, respectively. The residual deformation rate η of DG-2 was 8.11% higher than that of DG-1, which is attributed to the components, such as Guazi-Gong, Man-Gong, and Luohan-Fang. These components limit inter-layer slip of each component in the Dou-Gong model, maintaining its overall integrity and enhancing its stability.

Load-displacement Response of Constitutive Components

The load-displacement curves for the constitutive components of the Dou-Gong model under compression are shown in Fig. 13. The displacement of the component was calculated as the average value of the LDVTs on both sides, and the load was measured as the applied force by the testing machine. The results show that the deformation of the Dou-Gong models was concentrated mainly on the upper two floors when the specimen was installed upside down. Specifically, Lu-Dou component exhibited the highest vertical displacement, with DG-1 and DG-2 models reaching 23.00 mm and 24.12 mm, respectively, followed by Hua-Gong and the 2nd rise Hua-Gong. In DG-1, Ang and Shu-Tou components displayed relatively small vertical displacement, with the maximum displacement of less than 0.5 mm, which is significantly lower than that of DG-2. Furthermore, the displacement of Shu-Tou slightly decreased for both models after the load exceeded the yield load, primarily due to the compression of the middle part of Shu-Tou, followed by slight upward bending of the two ends with the gradual increase in load. After unloading, the residual deformation of Hua-Gong and Nidao-Gong components were obvious, whereas the residual deformation of the 2nd rise Hua-Gong in DG-1 was below 1 mm. The remaining components did not display any residual deformation, indicating that they were still in the elastic stage.

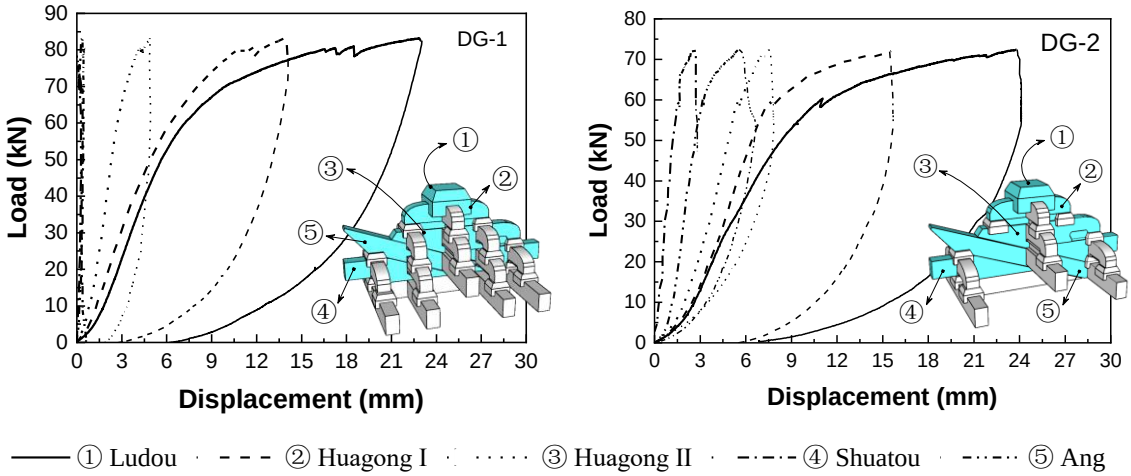

Fig. 13. Load-displacement curves of constitutive components

In the Dou-Gong model, the Ang component is unique due to its oblique placement, and the rationality of its placement depends on the relative slip value between Ang and adjacent components. In this study, the relative slip of Ang was defined as the slip of Ang relative to the 2nd rise Hua-Gong (LVDT 9 and 10). The load-relative slip curve of Ang is presented in Fig. 14. Initially, negligible or no relative slip was observed at the interface due to friction between the components. However, as the load increased, the load-relative slip curve of Ang displayed an approximate bilinear behavior, with slight slip observed in the second stage. After unloading, more than 60% of the slip did not return to the level prior to loading. For DG-1, the maximum relative slip between Ang and the 2nd rise Hua-Gong was 0.52 mm, which was less than 2% of the maximum vertical displacement of the top of the Lu-Dou (when the specimen is upside down), indicating the anchoring of the transverse arches and hidden dowel, as well as the friction of the contact surface effectively constrain the slip of Ang. Despite Ang cutting off the regular layering of Dou-Gong models, the Dou-Gong model maintains excellent vertical and horizontal stability. Conversely, for model DG-2, the maximum relative slip of Ang was 5.03 mm, significantly higher than that of DG-1, further demonstrating the efficacy of the transverse arches in limiting interlayer slip of each component in the Dou-Gong model.

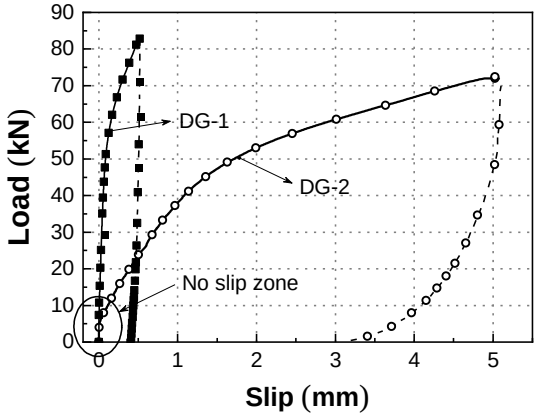

Fig. 14. Vertical load-slip curves

Load-strain Response

The strain of the lower surface of the Nidao-Gong, Hua-Gong, Man-Gong, and Ling-Gong in each specimen was obtained. As strain is directly proportional to the internal force of the components, the magnitude of strain can reflect the stress condition of the components. Figure 15 illustrates the load-strain curve of the Dou-Gong model. In both DG-1 and DG-2 models, the upper components (when the specimen is upside down) exhibited higher internal forces that were concentrated in the Nidao-Gong and Hua-Gong, which suggests that these components were subjected to the maximum vertical load. In contrast, the lower components exhibited lower internal forces, providing an explanation for the increased susceptibility of the upper components to damage while the lower components remained intact. During the elastic-plastic stage, the upper components, such as the Nidao-Gong and Hua-Gong, exhibited large tensile strains, which reflect the warping of these components due to cracking and deformation. The lower components primarily displayed compressive strain, indicating a lower probability of damage.

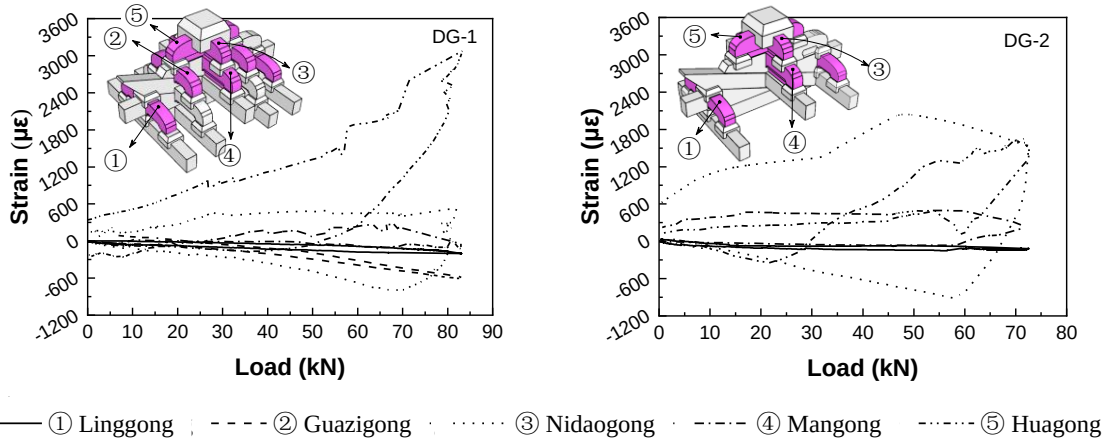

Fig. 15. Load-strain curves for Dou-Gong brackets

Mechanical Model of Vertical Load-Deformation

Based on the load-displacement curve (Fig. 11), it is apparent that the DG-1 and DG-2 models did not lose their bearing capacity due to the failure of a particular component during the loading process. Instead, the loss of bearing capacity was due to the perpendicular-to-grain compression yield of components, such as the Lu-Dou, resulting in a nonlinear hardening stage until the ultimate load was reached and the loading ceased. The mechanical behaviour of Dou-Gong model is highly similar to that of wood under compression perpendicular to the grain. Figure 16 depicts the stress-strain relationship of wood under compression and tension.

To facilitate theoretical analysis, the compressive bearing capacity of the Dou-Gong model was derived under two simplifying assumptions. Firstly, it was assumed that there were no machining errors or assembly clearances, and all contact surfaces were in complete and uniform contact. Secondly, given that the Lu-Dou was the first to yield under vertical loading, the deformation of the Dou-Gong model was considered as the sum of the compression deformation of the Lu-Dou and the upper structure above it. These assumptions served to simplify the theoretical analysis of the Dou-Gong model and provide a clearer understanding of its compressive bearing capacity. Based on these assumptions, it is possible to develop a geometric model for stiffness analysis of the Dou-Gong model, as illustrated in Fig. 17.

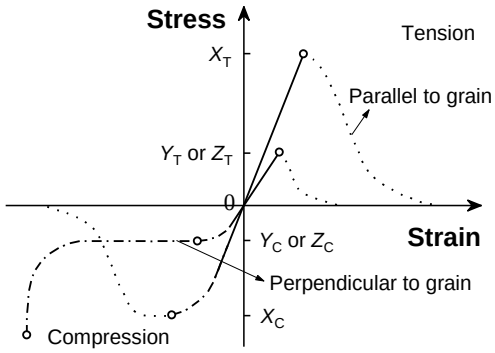

Fig. 16. Ideal elastic-plastic model of wood. Notes: In this figure, X_T denotes the tensile strength parallel to the grain; Y_T denotes the radial tensile strength perpendicular to the grain; Z_T denotes the tangential tensile strength perpendicular to the grain; X_C denotes the compressive strength parallel to the grain; Y_C denotes the radial compressive strength perpendicular to the grain; Z_C denotes the tangential compressive strength perpendicular to the grain.

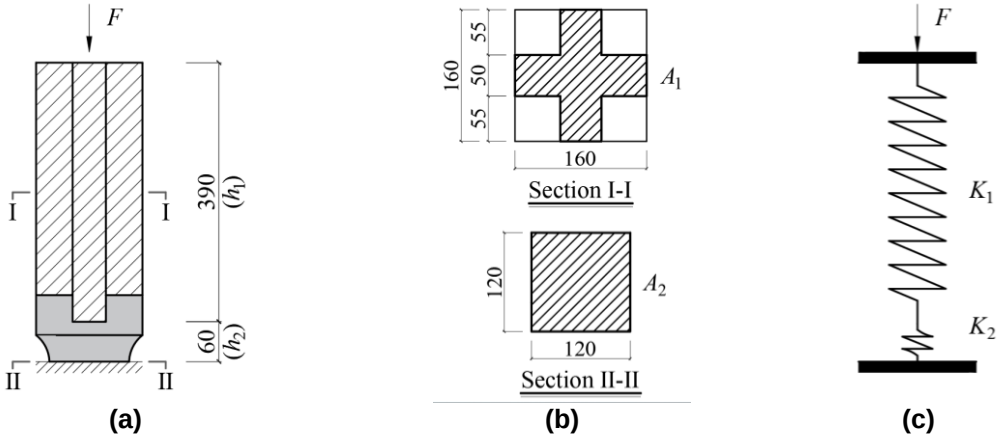

Fig. 17. Simplified models for calculating the stiffness of the Dou-Gong models under vertical load: (a) Model partitioning; (b) Compressive area; (c) Vertical spring system

The vertical stiffness is models as a dual-spring system in series along the vertical direction, *i.e.*, the stiffness K_1 of the upper structure and the stiffness K_2 of the lower structure (Lu-Dou) bounded by the contact interfaces between the Lu-Dou and the Nidao-Gong as well as the Hua-Gong. The stiffness can be calculated using Eqs. 2 and 3,

$$K_1 = \frac{E_{\perp} A_1}{h_1} \tag{2}$$

$$K_2 = \frac{E_{\perp} A_2}{h_2} \tag{3}$$

where $E_{\perp}$ denotes the elastic modulus of wood perpendicular to the grain (MPa). Considering the negative influence of wood defects on its strength and modulus of elasticity, the mechanical properties of wood are subjected to a reduction factor of 0.8 based on guidelines provided in the book of *Wood Structure Design Manual* (2021); A_1 denotes

the contact area between the upper structure and the Lu-Dou, with a value of 13500 mm^2; A_2 denotes the area of the compressed zone on the bottom surface of the Lu-Dou, with a value of 14400 mm^2; h_1 denotes the height of the upper structure, which is 390 mm. h_2 denotes the height of the lower structure, which is 60 mm.

Based on the vertical load tests conducted on the Dou-Gong model and its specific stress state, a bi-linear model for the vertical load-displacement response of the Dou-Gong model can be established, as shown in Fig. 18. The load-carrying capacity F of the Dou-Gong model under vertical load can be calculated using Eq. 4,

$$F = \begin{cases} K_e \Delta, & \left(0 \le \Delta \le \Delta_y\right) \\ F_y + K_p\left(\Delta - \Delta_y\right), & \left(\Delta_y \le \Delta\right) \end{cases} \tag{4}$$

where K_e denotes vertical stiffness of the elastic stage of the Dou-Gong model ($kN \cdot mm^{-1}$); K_p denotes the vertical stiffness of the elastic-plastic stage of the Dou-Gong model ($kN \cdot mm^{-1}$); F_y denotes the yield load of the 1:3.4 scaled Dou-Gong model (kN), defined as the yield load of the bottom surface of Lu-Dou, which leads to the transition of the Dou-Gong model into the elasto-plastic stage; Δ denotes the displacement in the direction of the applied force (mm); and Δ_y denotes the yield displacement (mm), which can be determined using Eq. 5 by considering the vertical displacement of the Dou-Gong model when the lower component (Lu-Dou) enters the non-linear hardening stage.

$$\Delta_y = \frac{f_{c\perp}}{E_\perp}\left(h_2 + \frac{h_1 A_2}{A_1}\right) \tag{5}$$

where $f_{c\perp}$ denotes the compression strength of wood perpendicular to the grain (MPa).

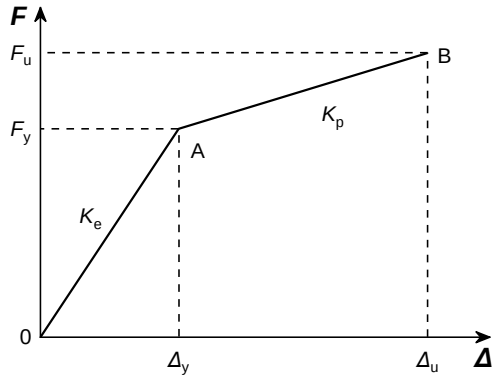

Fig. 18. Bi-linear curve of vertical load-displacement relationships for Dou-Gong brackets

Based on the results of material tests, the theoretical yield load of two Dou-Gong models was calculated to be 70.6 kN. The yield load test values for models DG-1 and DG-2 were 69.3 and 58.5 kN, respectively, with corresponding errors of 1.8% and 20.6% when compared with the theoretical values. The components of the Dou-Gong model are distributed in an umbrella shape in the vertical direction. This arrangement creates a situation that certain components experience eccentric compression due to the greater number of members present in lower layers (when the specimen is upside down). In particular, the lower components of the model DG-2 were subjected to more significant eccentric compression, resulting in the yield load test value of the Dou-Gong model being

lower than the theoretical value.

According to the deformable compatibility condition, the compression stiffness K_e of the Dou-Gong model in the elastic stage can be calculated by Eq. 6.

$$K_e = K_1 + K_2 = \frac{K_1 K_2}{K_1 + K_2} = \frac{EA_1 A_2}{h_1 A_2 + h_2 A_1} \quad (6)$$

In the elastic-plastic stage, the upper component of the structure remains its elastic behaviour, while the lower component undergoes plastic deformation. The stiffness K_p of the Dou-Gong model in the elastic-plastic stage can be calculated using Eq. 7,

$$K_p = \eta K_e \quad (7)$$

where η denotes the stiffness reduction factor. Based on the test results, a value of 0.14 can be adopted.

The vertical stiffness of the Dou-Gong model in the elastic stage, denoted as K_e, was calculated to be 6.53 kN·mm^{-1}, while in the elastic-plastic stage, the stiffness K_p was 0.91 kN·mm^{-1}, indicating a significant 86% stiffness reduction. The percentage errors between the theoretical and experimental values for K_{AB} in models DG-1 and DG-2 were found to be 5.8% and 20.6%, respectively, while those for K_{BC} were 5.7% and 20.4%, respectively. These results suggest that the adoption of a vertical spring model for calculating the vertical stiffness was a reasonable approach. Moreover, the bi-linear model was able to accurately reproduce the deformation behavior of the Dou-Gong model subjected to vertical loads. This finding is consistent with previous research (Gao 2007). Therefore, it is confirmed that the approach presented in this study is reliable and effective for modeling the Dou-Gong system under vertical loading conditions.

CONCLUSIONS

1. Under vertical load, Dou-Gong models exhibited failure primarily at the Lu-Dou, Nidao-Gong, and Hua-Gong. It is worth noting that Lu-Dou serves as a vulnerable component and tends to fail earlier than other components. It is suggested that the reinforcement strategies for Dou-Gong brackets subjected to external force should give priority to the study of these vulnerable components.
2. The Jixinzao and Touxinzao Dou-Gong models are characterized by marked plastic deformation features during the entire loading process, as evidenced by typical load-displacement curves with elastic and elastic-plastic stages. The Dou-Gong models demonstrated excellent load-bearing capacity and high deformation resistance. Notably, the Jixinzao Dou-Gong exhibited a 15.0% higher ultimate load-carrying capacity than the Touxinzao Dou-Gong, attributable to the transverse arches present in the former.
3. The Dou-Gong models displayed a positive correlation between the number of transverse arches and its compression stiffness, while the presence of transverse arches had a negligible effect on stiffness degradation rates. The Touxinzao Dou-Gong model exhibited superior ductility, characterized by a ductility coefficient 8.57% higher than that of the Jixinzao Dou-Gong model. The presence of transverse arches, including Guazi-Gong, Man-Gong, and Luohan-Fang, effectively limits interlayer sliding of

components in the Jixinzao Dou-Gong, thereby preserving its overall integrity and providing greater stability.

4. Although Ang disrupted the regular layering of the Dou-Gong models, both models exhibited exceptional overall stability in both the vertical and horizontal directions, with little interlayer sliding observed.
5. The bi-linear model can effectively simulate the deformation behaviour of the Dou-Gong model under vertical load.

ACKNOWLEDGEMENTS

This research is supported by the National Natural Science Foundation of China (Grant No. 51878345). Any research results expressed in this paper are those of the writer(s) and do not necessarily reflect the views of the foundations. The authors declare that they have no known competing financial interests or personal relationships that could have appeared to influence the work reported in this paper.

REFERENCES CITED

ASTM D143 (2014). "Standard test methods for small clear specimens of timber," ASTM International, West Conshohocken, PA.

Chen, M. D. (1991). *Ancient Chinese Wood Structure Building Technology (Warring States Period to Northern Song Dynasty)*," Cultural Relics Publishing House, Beijing, China.

Chen, Z. Y., Zhu, E. C., Lam, F., and Pan, J. L. (2014). "Structural performance of Dou-Gong brackets of Yingxian Wood Pagoda under vertical load - An experimental study," *Engineering Structures* 80, 274-288. DOI: 10.1016/j.engstruct.2014.09.013

Cheng, X. W., Shen, B., Liu, W. Q., Lu, W. D. (2019). "Experimental study on mechanical properties of Song-style Dou-Gong joints with Ang," *Journal of Building Structures* 40(04), 133-142. DOI: 10.14006/j.jzjgxb.2019.04.014

Fan, L. C., and Zhuo, W. D. (2001). *Ductile Seismic Design of Bridges*, Communications Press, Beijing, China.

Gao, D. F. (2007). *A Research on the Structure and their Aseismatic Characteristics of Ancient Chinese Timber Buildings*, Ph.D. Dissertation, Xi'an University of Architecture and Technology, Xi'an, China.

Gao, D. F., Zhao, H.T., Xue, J. Y., Zhang, P. C. (2003). "Experimental study on structural behavior of Dou-Gong under the vertical action in Chinese ancient timber structure," *Wood Earthquake Engineering* 19(3), 56-61.

Gao, Y., Xuan, S. Q., Xu, F. Y., Diao, Y., and Meng, X. M. (2022). "Shear performance of a novel non-metallic cross-laminated timber wall-to-wall connection using double-dovetail mortise-tenon joint," *Wood Material Science & Engineering*. DOI: 10.1080/17480272.2022.2101382

GB/T 1931 (2009). "Method of determination of the moisture content of wood," Standardization Administration of China, Beijing, China.

GB/T 1933 (2009). "Method of determination of the density of wood," Standardization

Administration of China, Beijing, China.
Li, J. (1982). *Yingzao Fashi*, China Architecture & Building Press, Beijing, China.
Liu, X. X., Lu, W. D., Cheng, X. W., and Wu, W. Q. (2021). "Research progress on mechanical properties of bracket set of traditional timber structures," *Journal of Nanjing Tech University (Natural Science Edition)* 43(03), 284-293. DOI: 10.3969/j.issn.1671-7627.2021.03.002
Liu, Y. Y., Han, Z. X., Tong, L. P., and Wang, W. H. (2020a). "Experimental study of mechanical performance of Dou-Gong in Mahavira Hall of Huishan Temple," *Journal of Tongji University (Natural science)* 48(04), 506-512. DOI: 10.11908/j.issn.0253-374x.19207
Liu, Y. Y., Zhang, F., Tong, L. P., and Wang, W. H. (2020b). "Experimental study on the Dou-Gong specimens of Huishan Temple under vertical loading," *Structural Engineers* 36(01), 130-135. DOI: 10.15935/j.cnki.jggcs.2020.01.018
Lu, W. D., and Deng, D. L. (2012). "Experimental research on seismic performance of wooden mortise-tenon joints before and after reinforcement," *Journal of Earthquake Engineering and Engineering Vibration* 32(3), 110-116. DOI: 10.13197/j.wwwv.2012.03.020
Ni, S. Z., and Li, Y. Z. (1994). "Investigation of wood species and analysis of main wood properties for traditional timber structures," *Building Science Research of Sichuan* (1), 11-14.
Pan, D. H. (2004). *Dou-Gong*, Southeast University Press, Nanjing, China.
Pan, Y., Yuan, S., Wang, H. Q., Wang, X. Y., and Lin, Y. J. (2017). "Numerical analysis of mechanical behavior of Tou-xin-zao and Ji-xin-zao tou-kung in Chinese ancient timber structures," *Journal of Civil and Environmental Engineering* 39(05), 9-15. DOI: 11835/j.issn.1674-4764.2017.05.002
Wang, H. Q. (2016). *Mechanical Behavior Analysis of Dou-Gong in Sichuan Ancient Timber Structures*, Master's Thesis, Southwest Jiaotong University, Chengdu, China.
Wang, T. (1992). *A Preliminary Study on the Static Force of Chinese Ancient Timber Structure*, Cultural Relics Publishing House, Beijing, China.
Wood Structure Design Manual (Fourth Edition) (2021). China Architecture & Building Press, Beijing, China.
Xu, B. H., Yu, K. B., Wu, H. C., and Bouchair, A. (2022). "Mechanical properties and engineering application potential of the densified poplar," *Wood Material Science & Engineering* 17(6), 659-667. DOI: 10.1080/17480272.2021.1924857
Xue, J. Y., Liang, X. W., Wu, C. W., Song, D. J., and Qi, L. J. (2022). "Experimental and numerical study on eccentric compression performance of Dou-Gong brackets at column tops," *Structures* 35, 608-621. DOI: 10.1016/j.istruc.2021.11.035
Yang, R. Y., Li, H. T., Lorenzo, R., Ashraf, M., Sun, Y. F., and Yuan, Q. (2020). "Mechanical behaviour of steel timber composite shear connections," *Construction and Building Materials* 258, article 119605. DOI: 10.1016/j.conbuildmat.2020.119605
Yang, R. Y., Mapesela, S., Li, H. T., and Lorenzo, R. (2023). "Mechanical properties of Dou-Gong bracket in Chinese traditional timber structure under vertical loads: A systematic review," *Journal of Building Engineering* 68, 106125. DOI: 10.1016/j.jobe.2023.106125
Yeo, S. Y., Komatsu, K., Hsu, M. F., and Que, Z. L. (2016). "Mechanical model for complex brackets system of the Taiwanese traditional Dieh-Dou timber structures," *Advances in Structural Engineering* 19(1), 65-85. DOI: 10.1177/1369433215618269

Yeo, S. Y., Komatsu, K., Hsu, M. F., Chung, Y. L., and Chang, W. S. (2018). "Structural behavior of traditional Dieh-Dou timber main frame," *International Journal of Architectural Heritage* 12(4), 555-577. DOI: 10.1080/15583058.2018.1442518

Yuan, X., Chen, Y. P., Tang, Q. H., and Guo, W. J. (2021). "Identification of common wood species of wooden components in ancient buildings based on micro-destructive testing," *Scientia Silvae Sinicae* 57(12), 122-131. DOI: 10.11707/j.1001-7488.20211212

Zheng, X. Z., Lam, F., Li, Z., and He, M. J. (2023). "Long-term performance assessment of post-tensioned timber connections under different climates," *Construction and Building Materials* 368, 130360. DOI: 10.1016/j.conbuildmat.2023.130360

Zhou, Q., Yan, W. M., Mu, C. X., and Yang, H. (2015). "Experimental investigation of bracket sets of 1st eave of Taihe Palace in the Forbidden City under vertical loads," *Journal of Southwest Jiaotong University* 50(05), 879-885. DOI: 10 3969/j.issn.0258-2724.2015.05.017

Zhou, Q., Yan, W. M., Mu, C. X., and Xie, Z. Q. (2017). "Experimental study of two-layer tou-kungs (wood brackets) from Taihe Palace in the Forbidden City under vertical loads," *Sciences of Conservation and Archaeology* 29(02), 8-14. DOI: 10.16334/j.cnki.cn31-1652/k.2017.02.002

Article submitted: July 14, 2023; Peer review completed: August 31, 2023; Revised version received: September 12, 2023; Accepted: September 13, 2023; Published: September 29, 2023.
DOI: 10.15376/biores.18.4.7745-7768